# Investigation of Electrical Behavior in Back Gated Graphene FET

**Rachid FATES [1] *, Toufik BENKEDIDAH [1], Riad REMMOUCHE [1], Jean-Pierre RASKIN [2]**

[1] *Department of Electronics, University of Mohamed Seddik Benyahia – Jijel, B.P. 98, Ouled Aissa, Jijel, 18000 Algeria*
[2] *Institute of Information and Communication Technologies, Electronics and Applied Mathematics, Université Catholique de Louvain, Place du Levant, 3, B-1348, Louvain-la-Neuve, Belgium*

http://doi.org/10.5755/j02.ms.41386

*Received 2 May 2025; accepted 12 June 2025*

New measurements of graphene ribbons allowed to highlight three electrical behaviors. We identified a mixed behavior consisting of a linear and a nonlinear trends. The measurements are associated with simulations in order to explain the charge carrier distribution in graphene and its impact on the transport in graphene devices. The results show the importance of the oxide doping and the minimum doping on the electrical activity of graphene. For the linear trend, a high and quite uniform doping is observed, around $10^{13}$ $cm^{-2}$. So, for the linear and the mixed trends, the doping change between $10^{11}$–$10^{12}$ $cm^{-2}$ and its distribution is localized close to the source and/or the drain terminals.
*Keywords:* graphene, ribbons, characterization, doping, behavior.

## 1. INTRODUCTION

A material with very high mobility is a major asset for the manufacturing devices operating at very high frequencies. This is why the scientific community has put a great deal of effort into producing graphene field effect transistors (GFETs). The graphene two-dimensional structure confers unique properties on the charge carrier motion, such as zero effective mass and ultra-relativistic behavior [1 – 3]. Because of these particularities, extraordinarily high intrinsic properties have been predicted theoretically and verified experimentally [4 – 6]. At the interface between semiconductor and metal, graphene was discovered experimentally by Geim and Novoselov in 2004. Its extraordinary electronic properties have been much talked about, above all they make it a promising candidate in the quest for the new electronics area [7 – 12].

In the literature, several works [13 – 19] have proposed analytical and numerical developments associated with experiments as a support to understand the operation of the graphene devices. In our previous work, we identified linear and nonlinear electrical behaviors in GFET at 300 K [20] and 77 K [21]. To our knowledge, few studies propose the modeling of the electrical behavior of graphene FETs. For example, the electrical behavior of GFET was attributed to metal-graphene contact in Ref. [22]. According to Zamzuri et al. [23], the linear and nonlinear behaviors in GFET are related to damage under electron irradiation. Otherwise, Martini et al. [24] attribute the electrical properties of GFET to the ribbon structure.

In addition to and in the light of what was reported previously, it is essential to find convergence in the explanation of electrical behavior in GFET devices. In this work, we identify another mixed behavior consisting of a linear and a nonlinear trends, and we use the simulation as a support for measurements to explain the divergence of electrical behavior. First, the scanning electron microscopy (SEM) pictures show the studied devices. The devices fabrication process and the measurements experimental setup are mentioned. Second, we introduce a theoretical model based on the small signal equivalent circuit of the back-gated graphene transistors in order to study the impact of the technological parameters on the electrical characteristics. Thus, the results suggest that the variation and the distribution of carrier density is relevant for electrical behaviors.

## 2. EXPERIMENT

Outlines of the fabrication process are described as follows: two-terminal graphene ribbon devices with a back gate are fabricated on a conventional silicon (Si) substrate covered by a 90 nm thick thermal silicon dioxide ($SiO_2$). Chemical vapor deposition (CVD) process is used for single-layer graphene deposition, then, the graphene layer is transferred onto the $SiO_2$/Si substrate. For the device fabrication, optical lithography is used for electrode patterns through a mask, and Ti/Au (10 nm/100 nm) metallic contacts are deposited by the thermal evaporator. In order to extract the electrical characteristics in the graphene ribbons, we performed measurements in vacuum on a lot of monolayer graphene transistors. The devices are 10 μm long by 16 μm wide, supported by $SiO_2$/Si substrate. In Fig. 1 a and b, a scanning electron microscopy (SEM) and an optical picture are shown, respectively. Advanced experimental details, measurements setup and methodology are reported in our previous studies [20, 21].

## 3. MODEL

The following model is inspired by the already existing studies on GFET and double gate GFET (DG-GFET) [11, 12]. Our approach is based on the extraction of an

* Corresponding author: R. Fates
E-mail: *rachid.fates@univ-jijel.dz*

equivalent small signal model of graphene ribbon in a back gate configuration.

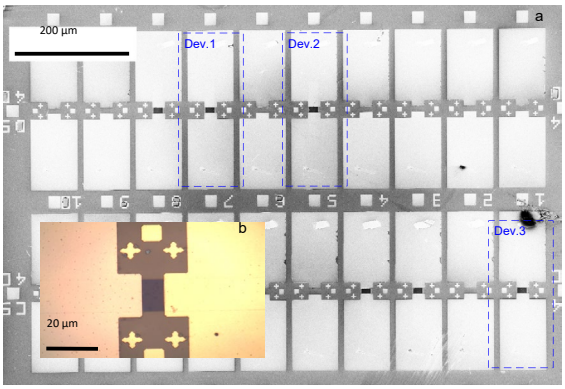


**Fig. 1.** Devices pictures: a – SEM image of the graphene ribbons devices; b – optical micrograph of one device

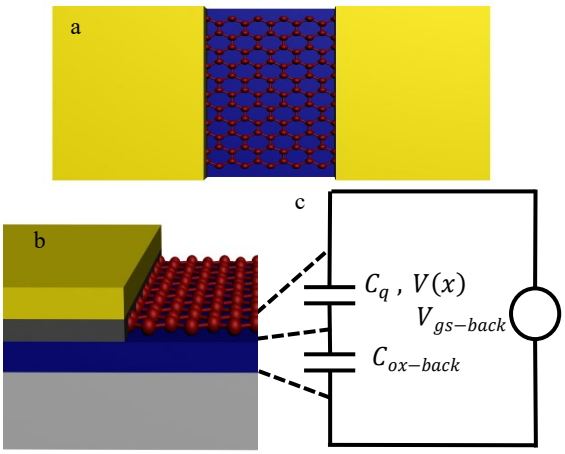


**Fig. 2.** Graphene ribbon device: a – top view; b – front view; c – small signal circuit

A schematic illustration of the small signal model is shown in Fig. 2 c. We also show a top view of the device in Fig. 2 a and a left view in Fig. 2 b.

First, the current expression is given as [11]:

$$I_{DS} = -q\,\mu W\left(\int_0^{V_{DS}} n_{rib}\,dV\right)\left(L-\mu\int_0^{V_{DS}}\frac{1}{v_{sat}}dV\right)^{-1}, \qquad (1)$$

where $q$ is the electron charge, $\mu$ is the carrier mobility, $W$ and $L$ are respectively the ribbon width and length, $v_{sat}$ is the carrier saturation velocity (= $10^6$ m/s), $V_{DS}$ the drain-source potential and $n_{rib}$ is the carrier density along the ribbon. The carrier density can be expressed as [2]:

$$n_{rib} = \frac{1}{q}\left|-\frac{1}{2}C_q\,V_{rib}\right| + n_{min}, \qquad (2)$$

with $n_{min}$ is the minimum carrier density pointing the charge neutrality point (CNP), $C_q$ is the quantum capacitance, introduced the first time by Fang et al. [25] for the semiconductors, it was defined as the derived of a local charge with respect to the associated electrostatic potential $V_{rib}$, thereafter, it was used for the graphene devices [11, 26, 27]. At zero band gap energy, the expression of the quantum capacitance as a function of the temperature $T$ and $V_{rib}$ is given as:

$$C_q = \frac{2q^2\,k_B\,T}{\pi(\hbar v_F)^2}\ln\left[2+2\cosh\left(\frac{qV_{rib}}{k_BT}\right)\right], \qquad (3)$$

where $k_B$ is the Boltzmann constant, $\hbar$ is the reduced Planck constant, and $v_F$ is the Fermi velocity. Applying the Kirchhoff law to the circuit described in Fig. 2 c, we can write $V_{rib}$ as follows:

$$V_{rib} = (V_{gs-back-eff} - V(x))\frac{C_{ox-back}}{C_{ox-back}+C_q}, \qquad (4)$$

where $C_{ox\text{-}back}$ is the gate oxide capacitance per unit area, the effective back gate voltage $V_{gs\text{-}back\text{-}eff} = V_{gs\text{-}back} - V_{gs\text{-}Dirac}$ with $V_{gs\text{-}Dirac}$ is the back gate voltage at the Dirac point, i.e. when the ribbon carrier density is reduced to $n_{min}$, and $V(x)$ is the potential evolution between the metallic contacts, from $L = 0$ to $L = 10$ µm, such as $V(L) = V_{DS}$.

## 4. RESULTS AND DISCUSSION

In order to simulate the output characteristics, we proceed first by identifying the technological parameter that controls the current slope, i.e. $n_{rib}$. According to Eq. 2, $n_{rib}$ depends on the gate oxide carrier density $C_qV_{rib}$ and the minimum carrier density $n_{min}$ resulting from the environment doping during the fabrication process. Then, when we apply the drain voltage, we study the local potential evolution along the ribbon from $x = 0$ to $x = L$. When the gate voltage is constant, $C_qV_{rib}$ depends only on the drain voltage. Since we cannot experimentally control the graphene ribbon carrier density profile, theoretically, this is equivalent to assume that $n_{min}$ does not have the same value along the ribbon, in these conditions, the $n_{rib}$ carrier density estimation is achieved by imposing a maximum convergence of the simulation to the current-voltage measurements. So, we developed a smart simulation algorithm that takes into account an adaptive convergence of the minimum carrier density values with respect to the potential evolution along the graphene ribbon, i.e., the algorithm fits the $n_{min}$ values to the measured data at each point along the ribbon. The results of the nonlinear behavior corresponding to device 1 (Dev. 1 in Fig. 1) are plotted in Fig. 3.

To have a clearer idea about the approach, we also plotted the output characteristics for a mean value of $n_{min}$ in Fig. 3 a. For the lower and higher values of $V_{gs}$, the simulated output characteristics and the corresponding carrier density profiles are plotted respectively in Fig. 3 c, d and e. In order to support this assumption, we assume that the graphene/Ti/Au contact is ohmic [28 – 31]. Otherwise, we get a good agreement between the simulations and measurements for the transfer characteristics plotted in Fig. 3 b, with a CNP around 38 V.

The carrier profiles in Fig. 3 d and e present the best approach to have a maximal convergence to the measured data. Fig. 3 d as well e shows two different profiles of $n_{min}$, the first one is a constant profile (equilibrium) and the second one is an adaptive or non-constant (non-equilibrium) profile, i.e. we don't have the same Fermi level anywhere in the ribbon area. To compare both cases, we can easily distinguish that the simulations in the non-constant profile present the best agreement with the measurements. By

analogy with Fig. 3 c, when combining Eq. 1 – Eq. 4, the evolution of $V(x)$ from the source to the drain reveals an interesting range of $0.6\ \text{V} < V_{ds} < 1.6\ \text{V}$ in which the corresponding values of $n_{min}$ change with the location in non-constant profile. These results could indicate that the ribbon lower carrier density regions act as a potential-barriers for electron motion.

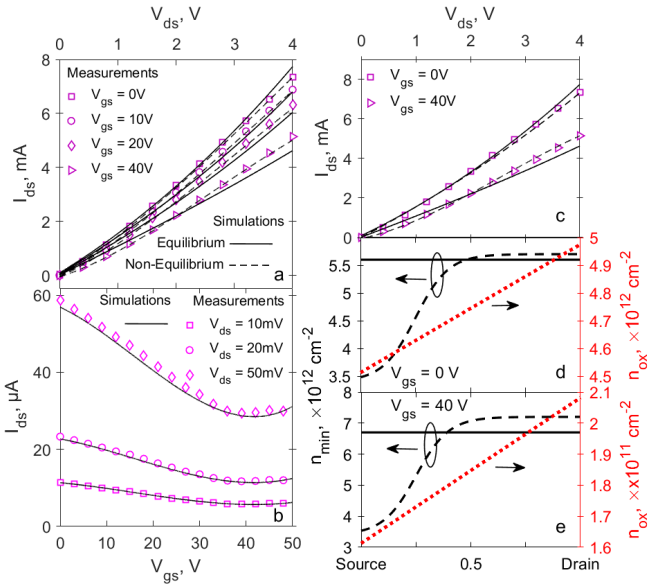


**Fig. 3.** Dev. 1 electrical characteristics: a – output characteristics for several $V_{gs}$ values; b – transfer characteristics for several $V_{ds}$ values. Symbols are measurements and lines are simulated curves; c – output characteristics with the associated carrier density profiles; d – $V_{gs} = 0$ V; e – $V_{gs} = 40$ V

For $V_{ds} \geq 1.6$ V, $n_{min}$ has a constant value and the current $I_{ds}$ has a linear trend. Two possible explanations could support this result: the carriers have enough energy to overcome the potential-barriers formed by the weakly doped locations, or, the electrons flow through a path where the doping is well distributed and/or almost uniform. From a physical point of view, for all $qV_{rib}$ energies at each point from $x = 0$ to $x = L$ that are greater than the thermal energy $KT$, the graphene ribbon is in the non-equilibrium regime, i.e. we don't have the same Fermi level anywhere in the ribbon area, so we don't have the same carrier density.

In Fig. 3 a, the simulations done for $V_{gs} = 40$ V show a significant difference between both curves associated to both $n_{min}$ profiles. Indeed, for the $n_{min}$ constant profile, the nonlinearity is less pronounced than the $n_{min}$ adaptive profile. This observation is not highlighted for $V_{gs} = 0$ V, where the difference between the simulated electrical curves corresponding to the two profiles is very slight, because of $n_{ox}$ range is comparable to the $n_{min}$ range, note that $n_{ox} = (1/q)\times|-0.5C_qV_{rib}|$ is the gate oxide carrier density. This result suggests there is a bond between the nonlinearity and the oxide charge density. From theoretical/simulation aspect, although the consideration of an average value of the density value is more often used, the results in Fig. 3 c, d and e demonstrate that the non-uniformity of the carrier density is in line with the experimental conditions, indeed, during the fabrication process, we have no control over the environmental doping of the graphene. For the second device (Dev. 2 in Fig. 1), a linear electrical behavior can be observed in Fig. 4 a. Experimentally, the CNP is situated beyond $V_{gs} = 60$ V, as shown in Fig. 4 b, so we cannot define the value of $n_{min}$ and the mobility.

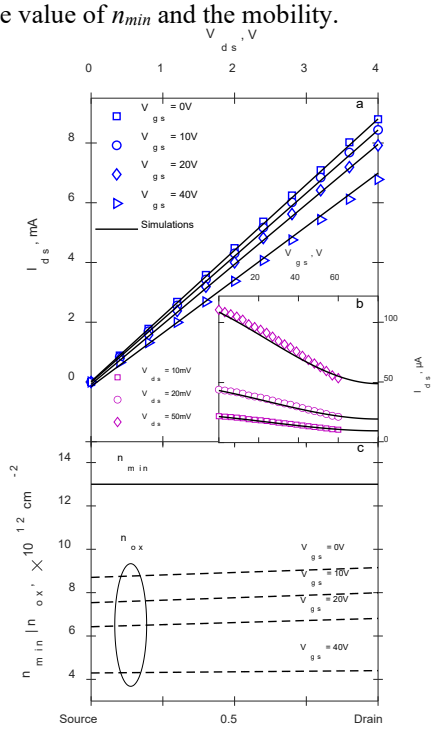


**Fig. 4.** Dev. 2 characteristics: a – output characteristics; b – transfer characteristics; c – the associated carrier densities profiles. Symbols are measurements and lines are simulations

Despite that, theoretically, we can optimize the simulation to get a good agreement with the measurements as shown in Fig. 4 a and 4 b, such as, CNP = 78 V, the mobility is 380 $\text{cm}^2/\text{Vs}$ and the carrier densities corresponding to $V_{gs}$ values are plotted in Fig. 4 c. Gradually, as the gate voltage increases, $n_{min}$ has a constant profile at $1.3 \times 10^{13}\ \text{cm}^{-2}$, while $n_{ox}$ profile decreases. For $V_{gs} = 0$ V, $n_{ox}$ changes from $8.7 \times 10^{12}\ \text{cm}^{-2}$ to $9.2 \times 10^{12}\ \text{cm}^{-2}$, which is more significant with respect to $V_{gs} = 40$ V, where $n_{ox}$ changes from $4.3 \times 10^{12}\ \text{cm}^{-2}$ to $4.5 \times 10^{12}\ \text{cm}^{-2}$. These variations could point the electrostatic field, as the gate voltage increases, the electrostatic field decreases and the gate field effect becomes dominant. In term of simulation, the main difference between the simulations done for Dev. 1 (Fig. 3) and Dev. 2 (Fig. 4) is identified by the CNP and $n_{min}$ values, and consequently $n_{rib}$, while the mobility plays a minor role. In summary, these results suggest that the carrier density in terms of concentration and profile plays an important role in the both electrical behaviors. In the literature, both of the nonlinear and linear behaviors were attributed to metal-graphene contact and the damage under electron irradiation [22, 23]. These two reasons contribute to the local doping of the graphene, which is in line with our results.

For the third device (Dev. 3 in Fig. 1), we get some kind of measurements describing a mixed electrical behavior. In Fig. 5 a, for $V_{gs} = 0$ V, we can identify two behaviors, a first one similar to a linear behavior for $V_{ds} < 1.4$ V and a second one looks like a reverse non-linear behavior for $V_{ds} > 1.4$ V. The carrier density changes from $1.1 \times 10^{12}\ \text{cm}^{-2}$ to $0.3 \times 10^{12}\ \text{cm}^{-2}$, as shown in Fig. 5 b. For $V_{gs} = 30$ V, at the

maximum value we could measure, we can identify three behaviors, a first one (I) similar to a linear behavior for $V_{ds} < 1$ V, a second (II) similar a reverse non-linear behavior for 1.2 V $\leq V_{ds} \leq$ 2.6 V, and a third behavior (III) describes a kink or an avalanche effect. The profiles associated with these three behaviors are summarized in Fig. 5 c and e. In Fig. 5 c, the carrier density changes from $1.25 \times 10^{12}$ cm$^{-2}$ down to $0.3 \times 10^{12}$ cm$^{-2}$ and increases thereafter from $0.3 \times 10^{12}$ cm$^{-2}$ up to $1 \times 10^{12}$ cm$^{-2}$ as $V_{ds}$ keeps rising. The comparison between Fig. 5 b and c could highlight the explanation of these behaviors. In Fig. 5 b, the non-constant profile associated to the reverse non-linear (semi-saturation) behavior could demonstrate that the graphene region close to the drain is less doped than the area near the source. In addition, the range of the $n_{ox}$, which changes from $4.8 \times 10^{12}$ to $5.2 \times 10^{12}$ cm$^{-2}$, is more important than the range of $n_{min}$ which plays a minor role and means that the electrostatic potential at the drain terminal has no significant effects.

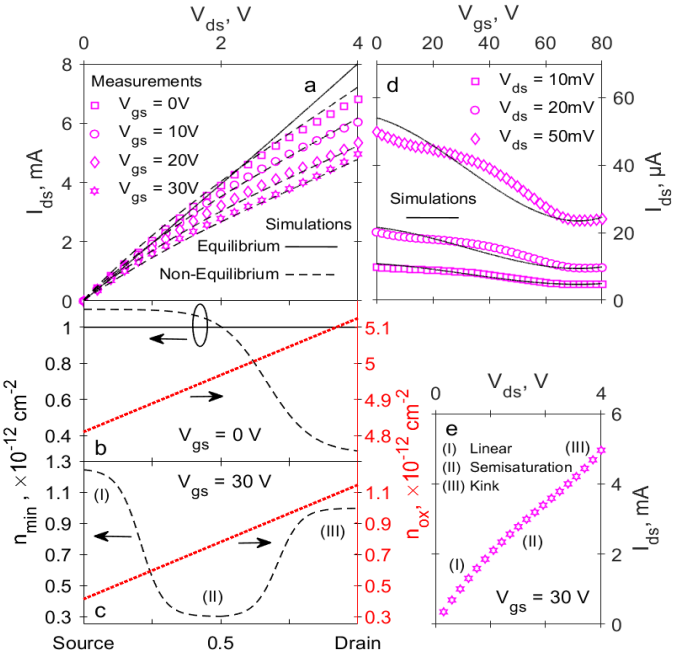


**Fig. 5.** Dev. 3 electrical characteristics: a – output characteristic. Symbols are measurements and lines are simulated curves; b, c – show the associated carrier density profiles; d – transfer characteristics; e – output characteristic measure-ments at $V_{gs} = 30$ V

In Fig. 5 c, the range is comparable to the $n_{min}$ range which could explain the increase of $n_{min}$ and contribute to the avalanche effect. Otherwise, in Fig. 5 d, the transfer characteristics show a good agreement with the measurements for $n_{min} = 1 \times 10^{12}$ cm$^{-2}$.

## 5. CONCLUSIONS

Three categories of electrical behavior in back-gated graphene ribbons are reported. The results show the importance of two relevant technological parameters: the oxide doping and the minimum doping on the graphene carrier density in terms of concentration and profile. For the linear trend, a high doping is observed over the graphene area, around $10^{13}$ cm$^{-2}$. For the nonlinear and the mixed trends, the doping change between $10^{11} - 10^{12}$ cm$^{-2}$ and its distribution is localized close to the source and/or the drain terminals. The comparison of our results for a constant and a non-constant profile with the literature shows that the local doping of the graphene is the origin of the behavior change.

## *Acknowledgments*

Our acknowledgements to the financial support from the Action de Recherche Concertées (ARC) "Naturist" project granted by the Communauté Fançaise de Belgique.

## REFERENCES

1. **Geim, A.K., Novoselov, K.S.** The Rise of Graphene *Nature Materials* 6 2007: pp. 183 – 191. https://doi.org/10.1038/nmat1849
2. **Meric, I., Han, M.Y., Young, A.F., Ozyilmaz, B., Kim, P., Shepard, K.L.** Current Saturation in Zero-Bandgap, Top Gated Graphene Field Effect Transistor *Nature Nanotechnology* 3 2008: pp. 654 – 659. https://doi.org/10.1038/nnano.2008.268
3. **Glazov, M.M., Ganichev, S.D.** High Frequency Electric Field Induced Nonlinear Effects in Graphene *Physics Reports* 535 2014: pp. 101 – 138. https://doi.org/10.1016/j.physrep.2013.10.003
4. **Neto, A.H.C., Guinea, F., Peres, N.M.R., Novoselov, K.S., Geim, A.K.** The Electronic Properties of Graphene *Reviews of Modern Physics* 81 2009: pp. 109 – 162. https://doi.org/10.1103/RevModPhys.81.109
5. **Fates, R., Remmouche, R., Benkedidah, T., Raskin, J.P.** Evolution of the Raman Spectra Features of Defective Monolayer Graphene in Back-Gate Configuration: Experimental Study *Diamond and Related Materials* 136 (6) 2023: 109919. https://doi.org/10.1016/j.diamond.2023.109919
6. **Rozhkov, A.V., Giavaras, G., Bliokh, Y.P., Freilikher, V., Nori, F.** Electronic Properties of Mesoscopic Graphene Structures: Charge Confinement and Control of Spin and Charge Transport *Physics Reports* 503 2011: pp. 77 – 114. https://doi.org/10.1016/j.physrep.2011.02.002
7. **Novoselov, K.S., Geim, A.K., Morozov, S.V., Jiang, D., Zhang, Y., Dubonos, S.V., Grigorieva, I.V., Firsov, A.A.** Electric Field Effect in Atomically Thin Carbon Films *Science* 306 (5696) 2004: pp. 666 – 669. https://doi.org/10.1126/science.1102896
8. **Fates, R., Bouridah, H., Raskin, J.P.** Probing Carrier Concentration in Gated Single, Bi- and Tri-layer CVD Graphene Using Raman Spectroscopy *Carbon* 149 (8) 2019: pp. 390 – 399. https://doi.org/10.1016/j.carbon.2019.04.078
9. **Urade, A.R., Lahiri, I., Suresh, K.S.** Graphene Properties, Synthesis and Applications: A Review *JOM* 75 2023: pp. 614 – 630. https://doi.org/10.1007/s11837-022-05505-8
10. **Mbayachi, V.B., Ndayiragije, E., Sammani, T., Taj, S., Mbuta, E.R., Khan, A.U.** Graphene Synthesis, Characterization and Its Applications: A Review *Results in Chemistry* 3 2021: pp. 100163. https://doi.org/10.1016/j.rechem.2021.100163
11. **Thiele, S.A., Schaefer, J.A., Schwierz, F.** Modeling of Graphene Metal-Oxide-Semiconductor Field-Effect Transistors with Gapless Large-Area Graphene Channels *Journal of Applied Physics* 107 2010: pp. 094505. https://doi.org/10.1063/1.3357398

12. **Landauer, G.M., Jiménez, D., González, J.L.** An Accurate and Verilog-A Compatible Compact Model for Graphene Field Effect Transistors *IEEE Transactions on Nanotechnology* 13 (5) 2014: pp. 895 – 904. https://doi.org/10.1109/TNANO.2014.2328782
13. **Frégonèse, S., Meng, N., Nguyen, H.N., Majek, C., Maneux, C., Happy, H., Zimmer, T.** Electrical Compact Modelling of Graphene Transistors *Solid-State Electronics* 73 2012: pp. 27 – 31. https://doi.org/10.1016/j.sse.2012.02.002
14. **Lv, Y., Huang, Q., Wang, H., Chang, S., He, J.** A Numerical Study on Graphene Nanoribbon Heterojunction Dual-Material Gate Tunnel FET *IEEE Electron Device Letters* 37 (10) 2016: pp. 1354 – 1357. https://doi.org/10.1109/LED.2016.2597155
15. **Shamloo, H., Nazari, A., Faez, R., Haji-Nasiri, S.** A Functional Study of a Bilayer Graphene Nanoribbon FET With Four Different Gate Insulators *IEEE Transactions on Nanotechnology* 18 2019: pp. 890 – 895. https://doi.org/10.1109/TNANO.2019.2936521
16. **Pasadas, F., Feijoo, P.C., Mavredakis, N., Pacheco-Sanchez, A., Chaves, F.A., Jiménez, D.** Compact Modeling Technology for the Simulation of Integrated Circuits Based on Graphene Field-Effect Transistors *Advanced Materials* 34 (48) 2022: pp. 2201691. https://doi.org/10.1002/adma.202201691
17. **Liana, Z., Choudhuri, B., Bhowmick, B.** Analytical Modeling of Drain Current for DG-Graphene Nanoribbon Vertical Tunnel FET *Microelectronics Journal* 147 2024: pp. 106194. https://doi.org/10.1016/j.mejo.2024.106194
18. **Rodriguez, S., Vaziri, S., Smith, A., Frégonése, S., Ostling, M., Lemme, M.C., Rusu, A.** A Comprehensive Graphene FET Model for Circuit Design *IEEE Transactions on Electron Devices* 61 (4) 2014: pp. 1199 – 1206. https://doi.org/10.1109/TED.2014.2302372
19. **Lu, N., Wang, L., Li, L., Liu, M.** A Review for Compact Model of Graphene Field-Effect Transistors *Chinese Physics B* 26 (3) 2017: pp. 036804 https://doi.org/10.1088/1674-1056/26/3/036804
20. **Fates, R., Raskin, J.P.** Linear and Non-Linear Electrical Behaviors in Graphene Ribbon Based Devices *Journal of Science: Advanced Materials and Devices* 3 (3) 2018: pp. 366 – 370. https://doi.org/10.1016/j.jsamd.2018.06.001
21. **Fates, R., Remmouche, R., Benkedidah, T.** Electrical Characteristics of Single Layer Graphene Ribbons in a Wide Temperature Range *Materials Science (Medžiagotyra)* 29(4) 2023: pp. 421 – 426. https://doi.org/10.5755/j02.ms.33700
22. **Wu, Y., Farmer, D.B., Xia, F., Avouris, P.** Graphene Electronics: Materials, Devices, and Circuits *Proceedings of the IEEE* 101 (7) 2013: pp. 1620 – 1637. https://doi.org/10.1109/JPROC.2013.2260311
23. **Zamzuri, A.S., Ayob, N.I., Abdullah, Y., Saidin, N.U., Che Hak, C.R.** Electrical Behavior of Graphene/$SiO_2$/Silicon Material Irradiated by Electron for Field Effect Transistor (FET) Applications *Materials Science Forum* 1010 2020: pp. 339 – 345. https://doi.org/10.4028/www.scientific.net/MSF.1010.339
24. **Martini, L., Chen, Z., Mishra, N., Barin, G.B., Fantuzzi, P., Ruffieux, P., Fasel, R., Feng, X., Narita, A., Coletti, C., Müllen, K., Candini, A.** Structure-Dependent Electrical Properties of Graphene Nanoribbon Devices with Graphene Electrodes *Carbon* 146 2019: pp. 36 – 43. https://doi.org/10.1016/j.carbon.2019.01.071
25. **Fang, T., Konar, A., Xing, H., Jena, D.** Carrier Statistics and Quantum Capacitance of Graphene Sheets and Ribbons *Applied Physics Letters* 91 (9) 2007: pp. 092109. https://doi.org/10.1063/1.2776887
26. **John, D.L., Castro, L.C., Pulfrey, D.L.** Quantum Capacitance in Nanoscale Device Modeling *Journal of Applied Physics* 96 (9) 2004: pp. 5180 – 5184. https://doi.org/10.1063/1.1803614
27. **Ammour, Y., Remmouche, R., Fates, R.** Modelling the Quantum Capacitance of Single-layer and Bilayer Graphene *Materials Science (Medžiagotyra)* 30 (1) 2024: pp. 3 – 7. https://doi.org/10.5755/j02.ms.34129
28. **Giubileo, F., Di Bartolomeo, A.** The Role of Contact Resistance in Graphene Field Effect Devices *Progress in Surface Science* 92 (3) 2017: pp. 143 – 175. https://doi.org/10.1016/j.progsurf.2017.05.002
29. **Chaves, F.A., Jiménez, D., Cummings, A.W., Roche, S.** Physical Model of the Contact Resistivity of Metal-Graphene Junctions *Journal of Applied Physics* 115 2014: pp. 164513. https://doi.org/10.1063/1.4874181
30. **Moon, J.S., Antcliffe, M., Seo, H.C., Curtis, D., Lin, S., Schmitz, A., Milosavljevic, I., Kiselev, A.A., Ross, R.S., Gaskill, D.K., Campbell, P.M., Fitch, R.C., Lee, K.M., Asbeck, P.** Ultra-Low Resistance Ohmic Contacts in Graphene Field Effect Transistors *Applied Physics Letters* 100 (20) 2012: pp. 203512. https://doi.org/10.1063/1.4719579
31. **Byun, K.E., Chung, H.J., Lee, J., Yang, H., Song, H., Heo, J., Seo, D.H., Park, S., Hwang, S.W., Yoo, I.K., Kim, K.** Graphene for True Ohmic Contact at Metal-Semiconductor Junctions *Nano Letters* 13 (9) 2013: pp. 4001 – 4005. https://doi.org/10.1021/nl402367y